Volume 10
Number 10
October 2025
Pages 2137–2622

Nanoscale Horizons

10 YEARS ANNIVERSARY

The home for rapid reports of exceptional significance in nanoscience and nanotechnology

rsc.li/nanoscale-horizons

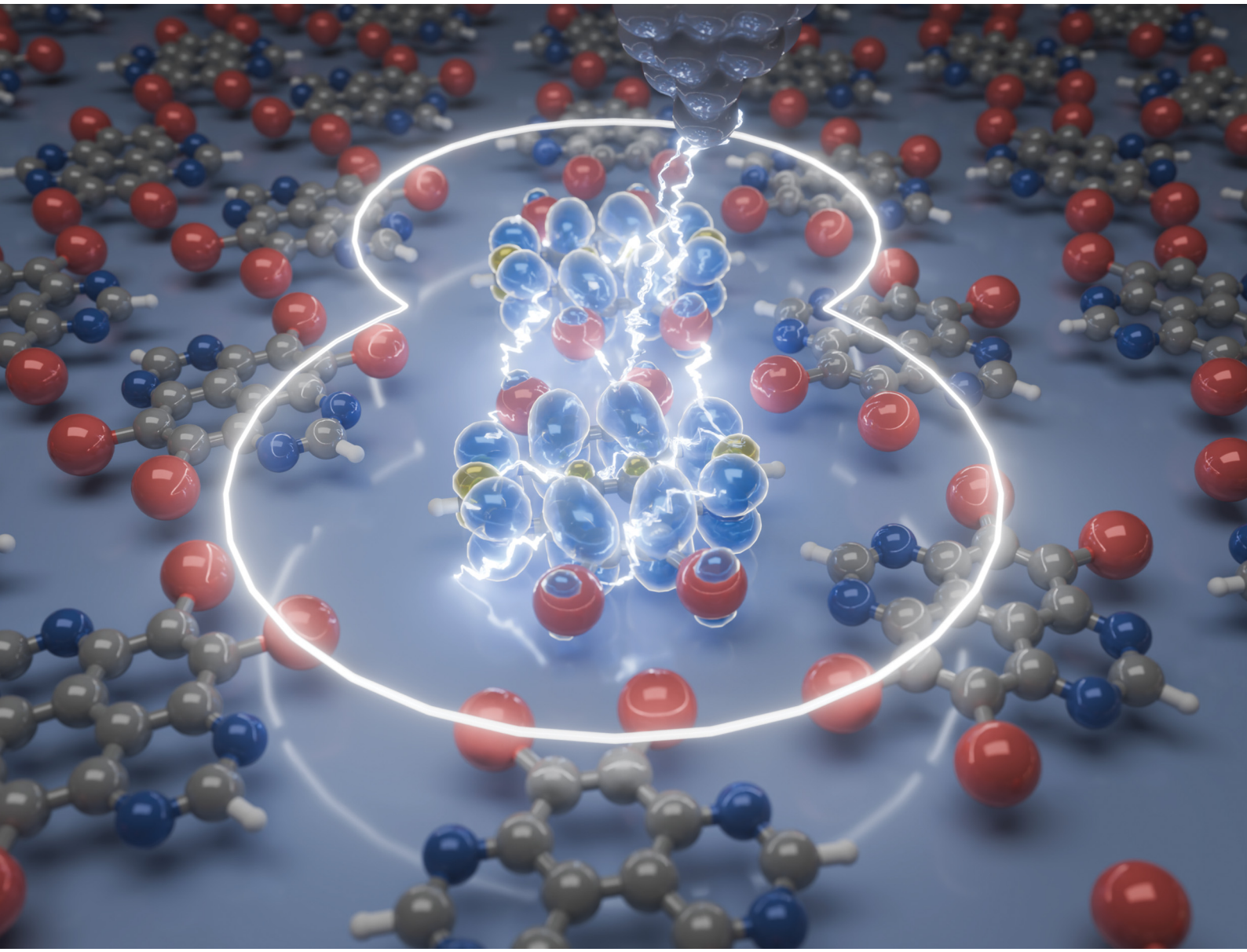

ISSN 2055-6756

ROYAL SOCIETY OF CHEMISTRY

COMMUNICATION
Shi-Xia Liu, Rémy Pawlak *et al.*
Discharge and electron correlation of radical molecules in a supramolecular assembly on superconducting Pb(111)

NCNST

Nanoscale Horizons

ROYAL SOCIETY OF CHEMISTRY

COMMUNICATION

View Article Online
View Journal | View Issue

Cite this: *Nanoscale Horiz.*, 2025, **10**, 2365

Received 4th July 2025,
Accepted 13th August 2025

DOI: 10.1039/d5nh00462d

rsc.li/nanoscale-horizons

Discharge and electron correlation of radical molecules in a supramolecular assembly on superconducting Pb(111)

Carl Drechsel,[a] Chao Li,[a] Jung-Ching Liu,[a] Xinyi Liu,[b] Robert Häner,[b] Silvio Decurtins,[b] Ulrich Aschauer,[c] Shi-Xia Liu,*[b] Ernst Meyer[a] and Rémy Pawlak*[a]

Precise control over the charge-state of radical molecules on surfaces is essential for engineering correlated electronic states in nanoscale architectures. Here, we demonstrate the supramolecular assembly of tetraazapyrene-based radicals on superconducting Pb(111), where anionic species formed through charge transfer from the substrate coexist with their neutral counterparts. These radicals can be discharged *via* capacitive coupling with the local electric field of the scanning probe tip, producing peaks (dips) in tunneling (force) spectra. Spatial mapping further reveals cascade discharging events and electron correlation between adjacent molecules of the lattice. Through tip-induced debromination, we achieve irreversible discharge enabling the creation of defect patterns. Our results establish a pathway towards gate-tunable spin arrays with ultra-high areal density, leveraging charge-state control and emergent electron correlations in molecular assemblies.

New concepts

Electron spin lattices on superconductors offer a promising platform for quantum technologies. They can serve as qubits in quantum computing or provide a basis for exploring exotic quantum phases, such as spin liquids and topological superconductivity. However, constructing and scaling up these artificial lattices while maintaining precise gate tunability remains a significant experimental challenge. In our work, we demonstrate the supramolecular assembly of 4,5,9,10-tetrabromo-1,3,6,8-tetraazapyrene (TBTAP) molecules on a superconducting Pb(111) surface, forming a compact electron (spin) superlattice consisting of coexisting neutral TBTAP and singly charged $TBTAP^{\bullet -}$ species. Using tunneling and force spectroscopy, we identify the signature of a discharging event in the charged $TBTAP^{\bullet -}$ molecules. This event is triggered by capacitive coupling between the molecular charge state and the local electric field from the STM/AFM tip, enabling a controlled transition from the anionic to the neutral state as a function of the applied tip voltage. Our results demonstrate a new pathway for the bottom-up construction of gate-tunable, high-density spin networks, offering a powerful platform for investigating electron correlation effects and emergent quantum phenomena at the molecular scale.

Introduction

Interacting electrons on a lattice are ubiquitous and can develop strong quantum correlations, which are at the basis of many intriguing many-body ground states such as unconventional superconductivity,[1] metal–insulator transitions, topological phases,[2–4] or magnetism.[5] Periodic arrangements of quantum dots (QD), whose electron (spin) occupancy can be tuned by an external electric field, can host such correlated states due to the competition between on-site Coulomb interaction U (the energy to add/remove an electron to the QD) and hopping amplitude t described by the Hubbard model. Various experimental platforms have been explored for realizing such fermionic Hubbard systems in optical lattices,[6,7] moiré superlattices,[1–4,8,9] and semiconductor quantum dot arrays.[5,10,11] Engineering correlated states must combine both an atomic-scale positioning of QDs into a well-defined lattice with a fine tuning of their charge-state individually and independently.[12,13] However, upscaling these artificial lattices while keeping a fine control over the gate tunability still remains a challenging experimental task.

Scanning tunneling microscopy (STM) and atomic force microscopy (AFM) are particularly suitable techniques not only to probe the local density of states (LDOS) at the nanoscale but also to tailor complex atomic/molecular structures at surfaces using manipulation techniques.[14] Quantum dot lattices have been already realized by implanting one-by-one phosphorous dopants in silicon using a STM, allowing simulations of prototypical Mott-insulator physics.[9–11,15] The tip of a STM/AFM microscope can also act as a local gate, enabling the detection

[a] *Department of Physics, WSS-Research Center for Molecular Quantum Systems, University of Basel, Klingelbergstrasse 82, 4056 Basel, Switzerland. E-mail: remy.pawlak@unibas.ch*
[b] *Department of Chemistry, Biochemistry and Pharmaceutical Sciences, W. Inäbnit Laboratory for Molecular Quantum Materials and WSS-Research Center for Molecular Quantum Systems, University of Bern, Freiestrasse 3, 3012 Bern, Switzerland. E-mail: shi-xia.liu@unibe.ch*
[c] *Department of Chemistry and Physics of Materials, University of Salzburg, Jakob-Haringer-Strasse 2A, 5020, Salzburg, Austria*

and manipulation of elementary charges with single-electron precision within individual atoms, molecules or QD.[16–24] Tip-assisted charging/discharging at such fundamental level has unveiled electron-transfer processes between isolated molecules[25–27] or multiple charging.[28,29] With the prospects of creating large QD arrays at surfaces, we propose an alternative approach based on radical molecules at surfaces whose integer charge-state can be controlled by tip gating.[19,30] Molecules can spontaneously assemble into complex supramolecular networks whose structures depend on the subtle balance between molecule–substrate and intermolecular interactions.[31] Their great versatility in terms of chemical design also allows the introduction of donor and electron acceptor groups,making organic molecules prime candidates for use as quantum bits.[32]

In a recent work, we demonstrated that single 4,5,9,10-tetrabromo-1,3,6,8-tetraazapyrene (TBTAP) molecules when directly adsorbed on both Ag(111) and Pb(111) surfaces systematically reach an anionic state through charge transfer,[19,33] making them excellent candidates for investigating electron–electron interactions within complex structures. When short chains are constructed on Pb(111) by tip manipulation, Coulomb repulsion introduces an alternation of charged and neutral molecules along the chain which can be switched due to strong capacitive coupling effectively implementing a molecular memory device.[33]

Here, we report on the formation of an extended array of radical TBTAP$^{\bullet-}$ molecules (Fig. 1a) on superconducting Pb(111) using low temperature STM and density functional theory (DFT) calculations. Upon adsorption, neutral and singly-charged TBTAP molecules coexist in the assembly arranged into adjacent rows of charged (c) and neutral (n) molecules. Using differential conductance measurements dI/dV(V) and force-voltage spectroscopy $\Delta f(V)$, we show the signature of the discharging event of the charged TBTAP$^{\bullet-}$ molecules triggered by a capacitive coupling with the electric field of the STM/AFM tip, allowing a transition from anionic to neutral state as a function of tip voltage. Spatial mapping reveals Coulomb rings centered on each molecular unit due to their electrical discharge. The rings evolve to a fused pattern at higher gating voltages, which is the manifestation of cascade

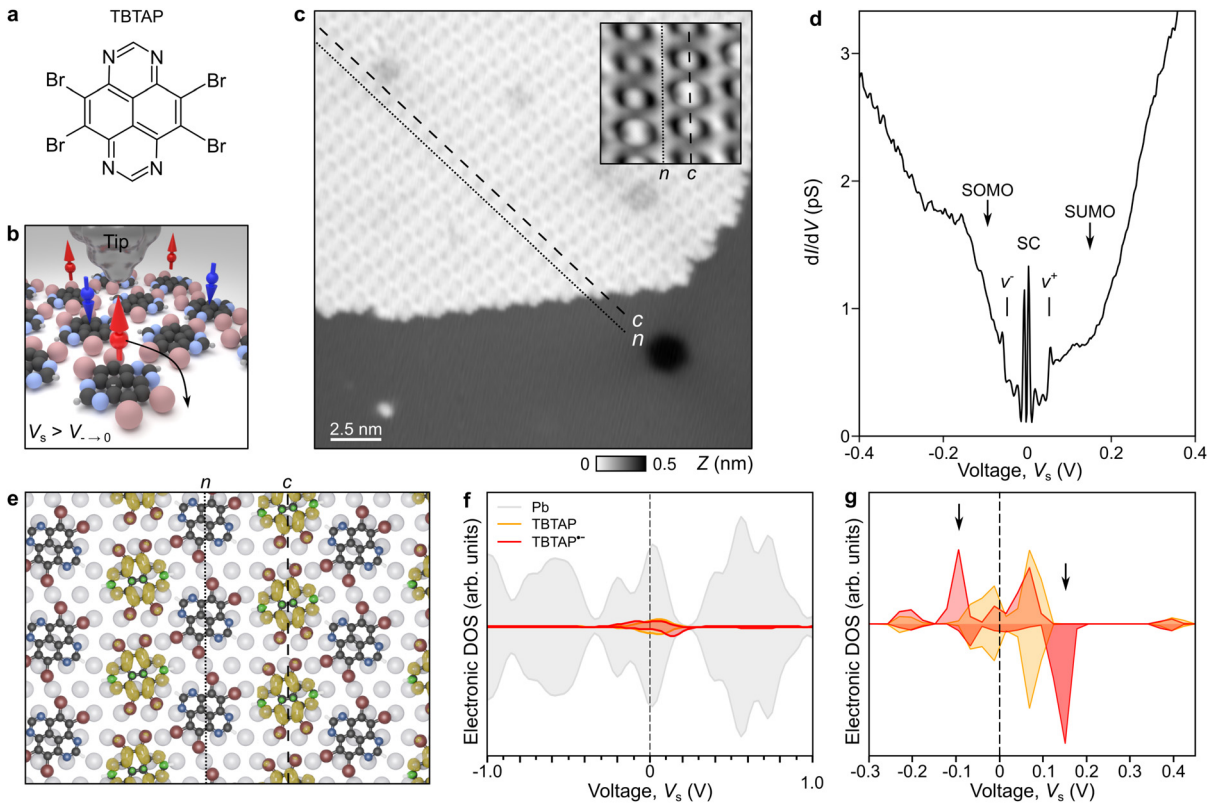

Fig. 1 Supramolecular assembly of radical TBTAP$^{\bullet-}$ on superconducting Pb(111). (a) Chemical structure of the TBTAP precursor. (b) Schematic of the experiment: TBTAP molecules assemble into a lattice of charged and neutral molecules. When the tip voltage V_s exceeds $V_{-\to 0}$, the local electric field acts as an external gate enabling the discharge of radical TBTAP$^{\bullet-}$ molecules. (c) STM overview of the supramolecular assembly on Pb(111) (V_s = 50 mV, I_t = 1 pA). The dashed and dotted lines labeled c and n correspond to rows of charged and neutral TBTAP molecules. The inset is a STM images of the lattice at V_s = 1 V. (d) Representative dI/dV point-spectra of a TBTAP$^{\bullet-}$ molecules (lock-in parameters: f = 611 Hz, A_{mod} = 800 μV). Peaks labeled SC refers to the Pb superconducting gap while $\nu_\pm$ are vibrational resonances of the radical TBTAP$^{\bullet-}$. SOMO and SUMO refers to the singly occupied molecular orbital and singly unoccupied molecular orbital. (e) Spin density of the charged lattice shown in a 2 × 2 supercell as calculated by DFT. Black, blue, red and gray colors refer to C, N, Br and Pb atoms. TBTAP$^{\bullet-}$ molecules are displayed with their spin density (positive: yellow, negative: green). (f) Electronic density of states showing contributions from the Pb surface (gray) as well as the charged (TBTAP$^{\bullet-}$) and the neutral (TBTAP) molecule. (g) Zoon-in on the electronic density of states near the Fermi level of the TBTAP$^{\bullet-}$ (red) and the neutral TBTAP (yellow) molecules.

discharge between the molecules and the electron correlation in the superlattice.

Methods

Sample preparation

A Pb(111) single crystal was cleaned by several sputtering and annealing cycles in ultra high vacuum. TBTAP molecules[34] were sublimated in ultra-high vacuum (UHV) from a quartz crucible heated at 180 °C onto the sample kept at about 250 K.

STM/AFM experiments

The experiments were performed using a low-temperature STM/AFM microscope operated at T = 4.8 K in ultrahigh vacuum ($p \approx 1 \times 10^{-10}$ mbar). The force sensor is a tuning fork based on a qPlus design[35] operated in the frequency-modulation mode (resonance frequency $f_0 \approx 25$ kHz, spring constant $k \approx 1800$ N m^{-1}, quality factor $Q \approx 14\,000$ and oscillation amplitude $A \leq 1$ Å). The bias voltage was applied to the tip. STM images are taken in constant-current mode. AFM measurements were acquired in constant-height mode at V = 0 V. The tip mounted to the qPlus sensor consists in a 25 μm-thick PtIr wire, shortened and sharpened with a focused ion beam. A clean and sharp Au tip was then prepared at low temperature by repeated indentations into the surface. Scanning tunneling spectroscopy (STS) data acquired at low temperature with the lock-in technique at 4.8 K (A_{mod} = 15 meV, f = 531 Hz).

Differential conductance spectroscopy dI/dV(V) spectra were acquired with superconducting tips at the University of Basel with a custom-made Joule-Thomson STM/AFM microscope. The microscope equipped with a 2.2 T dry magnet operates at 1.0 K with a SPECS-Nanonis RC5e electronics. STM tips were made from a 250 μm-thick Pb wire, which were sputtered for 2–3 hours in UHV to remove its native oxide. A superconducting tip was then prepared by repeated indentations into a clean Pb surface until a good superconducting gap is obtained. dI/dV spectra are acquired with the lock-in amplifier technique using a modulation of 610 Hz and a modulation amplitude of 15–50 μeV.

DFT calculations

DFT calculations for Pb(111)-adsorbed molecules were performed using the Quickstep code[36] within the CP2K package,[37] employing a mixed Gaussian-planewave basis. The revPBE[38] density functional was employed in all calculations together with the Grimme-D3 correction[39] for van-der-Waals interactions. We used a molecularly optimized shorter range double zeta atomic basis[40] together with Goedecker–Teter–Hutter pseudopotentials,[41] employing 4, 5, 4, 1 and 7 valence electrons for Pb, N, C, H and Br respectively. Calculations with single molecules were performed on 6 × 6 supercells of the Pb(111) surface slab with 4 atomic layers. Calculations for the assembled monolayer were performed in the supercell with lattice parameters 12.125 Å × 19.489 Å and a cell angle of 98.948° with 4 atomic layers as used in our previous study.[42] Structures were relaxed until forces converged below 4.5 × 10^{-4} Hartree per Bohr. While charging of the TBTAP molecules occurred spontaneously, this charging was controlled by inducing local magnetic moments on atoms of the different molecules.

Results and discussion

Supramolecular electron spin lattice on Pb(111)

TBTAP molecules were sublimated on a Pb(111) surface kept below room temperature ($T \approx 250$ K) leading to the formation of large molecular islands (Fig. 1c). STM imaging reveals a densely packed rectangular lattice showing alternating bright and dark rows (see inset of Fig. 1c). These two contrasts are observed across different rows, labeled as c (dashed line) and n (dotted line), which corresponds to rows of charged and neutral molecules, respectively.[42] Fig. 1b depicts the experiment, which aims at the controlled discharge of individual TBTAP$^{\bullet-}$ molecules (represented by red and blue dots/arrows) by the local electric field of the probing tip. The discharge is obtained by applying a potential difference between tip and sample such as the sample voltage V_s is greater than the threshold voltage V_{Thresh} required for the molecule's discharge. As we described in a recent work,[42] DFT calculations conclude that molecules self-assemble through hydrogen-hydrogen and halogen–halogen bonding between the peripheral Br atoms and the tetraazapyrene moieties (Table 1). The densely packed rectangular structure is in registry with the Pb lattice (Fig. 1e) with lattice parameters a_1 = 12.12 Å and b_1 = 19.48 Å. These values are comparable to the experimental STM images with lattice parameters a_1 = 12.3 Å and b_1 = 18.2 Å. The two TBTAP charge states are observed by STM imaging as dark and bright contrasts for charged (c) and neutral (n) molecules, which are systematically located in rows labeled by dotted lines and dashed lines in Fig. 1. The charged array is also confirmed by DFT calculations of Fig. 1e, in which anionic TBTAP$^{\bullet-}$ are identified by their non-zero spin density.

Charge-state control of anionic TBTAP$^{\bullet-}$ with the electric field of the tip

Anionic TBTAP$^{\bullet-}$ molecules are spontaneously obtained by the transfer of a single electron from the Pb(111) surface to the lowest unoccupied molecular orbital (LUMO) of the neutral TBTAP upon adsorption. During this charging, the LUMO occupied by one electron falls below the Fermi level E_F, splits into a singly occupied molecular orbital (SOMO) of spin 1/2 below E_F and a singly unoccupied molecular orbitals (SUMO) above E_F.[19,30,43] Fig. 1d shows an experimental dI/dV(V) point-spectrum acquired on a TBTAP$^{\bullet-}$ molecule. Peaks labeled SC

Table 1 Parameters of the supramolecular lattice extracted from DFT calculations

	Values in Å
Lattice parameters (a_1, b_1)	12.19, 19.48
Br–Br bond length	3.8-4.0
Hydrogen bond length	≈ 2.5

indicate the edges of the superconducting gap while $\nu_{\pm}$ corresponds to vibrational excitations of TBTAP$^{\bullet-}$ molecules.[19] Since each TBTAP$^{\bullet-}$ molecule carries an electron spin, they give rise to Yu–Shiba–Rusinov (YSR) in-gap states by interacting with the superconducting state, which we have characterized in details in previous works.[19,33] Fig. 1f and g show DFT calculations of the electronic density of states (DOS) for the neutral TBTAP (yellow) and radical TBTAP$^{\bullet-}$ (red). The spin asymmetry of TBTAP$^{\bullet-}$ as compared to the neutral TBTAP is clearly visible around E_F since the up-spin channel has occupied DOS while the down-spin channel is mostly empty. Note also that DFT calculation predicts anionic TBTAP$^{\bullet-}$ on Pb(111) to be 7.95 meV more stable than the neutral TBTAP. In the enlarged spectra of Fig. 1g, an additional up-spin occupied state is observed at 0.1 eV below E_F for the TBTAP$^{\bullet-}$ and the unoccupied counterpart (down-spin) at 0.15 eV above E_F (black arrows). These energies are comparable with the onset of the two shoulders at −100 and +150 meV observed in dI/dV spectra (Fig. 1d), which could be ascribed to the SOMO and SUMO levels of the TBTAP$^{\bullet-}$ molecules on Pb(111).[19]

The experimental signature of the TBTAP$^{\bullet-}$ discharge in dI/dV maps is the observation of dots/rings (peaks) of high-conductance centered to the TBTAP$^{\bullet-}$ molecules (Fig. 2a and b). The discharge of the TBTAP$^{\bullet-}$ radical is described using the model of a double barrier tunneling junction (DBTJ) (Fig. 2c and d).[30] The threshold voltage for the discharge depends on the gating efficiency of the tip represented by the lever arm α. The energy shift ΔE of the SOMO level directly depends on α by the equation $\Delta E = e\alpha V$ (with e the elementary charge).[44] Since the discharge is governed by a capacitive coupling between tip and molecule, α linearly depends on V as well as on the (X, Y, Z) positions of the tip with respect to the anionic molecule. The estimation of α is obtained from the ratio between the occupied SOMO level of the molecule (E_{SOMO}) and the energy of the discharge $E_{-\rightarrow 0} = eV_{-\rightarrow 0}$ such as $\alpha = E_{SOMO}/(E_{-\rightarrow 0})$.[30] Since E_{SOMO} equals to ≈ -180 meV (Fig. 1d and g) and $E_{-\rightarrow 0} \approx 0.9$ eV, the value of α is 0.15–0.2, which is comparable with previous works on the discharge of molecules on metals[30] or on thin insulating layers.[26]

Ramping up the voltage between tip and sample leads to the increase of the local electric field of the tip, which shifts the chemical potential of the substrate μ_s by ΔE towards the SOMO level (Fig. 2c). When $V_s \geq V_{-\rightarrow 0}$, the SOMO level aligns with μ_s and becomes empty by the transfer of its electron back to the substrate (black arrow in Fig. 2c). As a result, the molecule undergoes a charge-state transition from the anionic TBTAP$^{\bullet-}$ to the neutral TBTAP^0 counterpart at the threshold voltage $V_{-\rightarrow 0}$. The constant-height dI/dV(X, Y) map of Fig. 2b acquired at constant positive sample voltage V_s such as $V_s \geq V_{-\rightarrow 0}$ then shows the discharge as dots/rings of high conductance

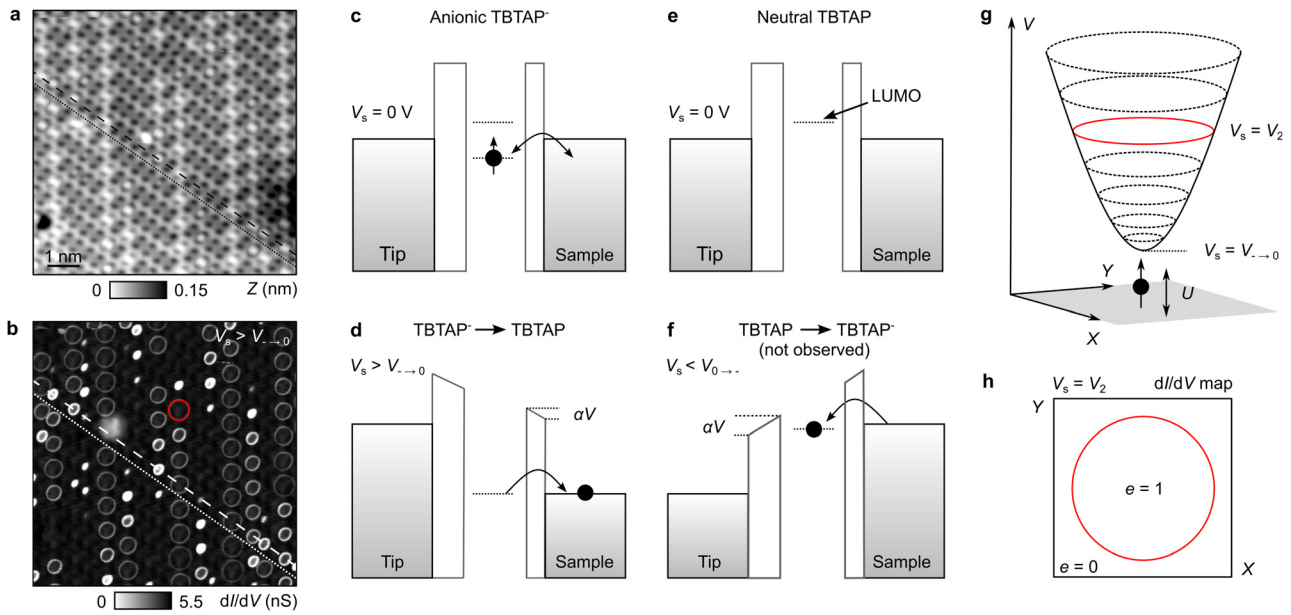

Fig. 2 Discharge rings from radical TBTAP$^{\bullet-}$ in STS maps. (a) STM image of the assembly (I_t = 1 pA, V_s = 1.3 V) and (b) corresponding dI/dV(X, Y) map showing rings of high conductance due to the discharge of TBTAP$^{\bullet-}$ molecules (lock-in parameters: f = 510 Hz, A_{mod} = 10 mV). The dashed and dotted lines labeled c and n correspond to rows of charged and neutral TBTAP molecules. (c) Schematic of the DTBJ model of the TBTAP$^{\bullet-}$ without the electric field of the tip (V_s = 0 V). TBTAP$^{\bullet-}$ molecules are occupied by a single electron transferred from the substrate into the SOMO. (d) When $V_s \geq V_{-\rightarrow 0}$, the SOMO level shifted by $\Delta E = \alpha V$ aligns with the substrate chemical potential μ_s, leading to the transfer of the electron back to the substrate (black arrow). This corresponds to the charge-state transition of the TBTAP$^{\bullet-}$ from anionic to neutral. (e) Schematic of the neutral TBTAP without the electric field of the tip, having its LUMO above the Fermi level. (f) When $V_s \leq V_{0\rightarrow -}$, the substrate chemical potential μ_s might align with the LUMO leading to the transfer of an electron from the substrate to the LUMO of the molecule (black arrow). This charge-state transition of TBTAP molecule from neutral to anionic was not observed experimentally in the assembly. (g) TBTAP$^{\bullet-}$ mimics a singly-occupied QD with on-site Coulomb interaction U. Scanning at constant height Z with voltages $V_s \geq V_{-\rightarrow 0}$ leads to the molecule's discharge when the tip is located above the molecule. (h) Dot/rings appear in dI/dV(X, Y) map which diameters depend on V_s. Inside such ring, the tip efficiently gates the molecule provoking the removal of its electron (e = 1).

centered to the position of the TBTAP$^{\bullet -}$ molecule. The center of the ring also pinpoints the position of TBTAP$^{\bullet -}$ molecules (see red ring) where the charge was located prior to its removal. Conversely, the application of negative sample voltage may induce the charging of neutral TBTAP when $V_s \leq V_{0\rightarrow -}$ with $V_{0\rightarrow -}$ is the threshold voltage to induce the charge-state transition from neutral to anionic. This is obtained by shifting the substrate chemical potential μ_s as described in Fig. 2f, in order to fill the LUMO orbital with an electron from the substrate.

The appearance of ''Coulomb'' rings is described in Fig. 2g and h for anionic TBTAP$^{\bullet -}$, respectively. Each charge molecule behaves as a Coulomb-blockaded molecular quantum dot with on-site Coulomb interaction energy U. The paraboloid centered to the QD represents the discharge. When the tip scans the molecule at constant-height Z for $V_s = V_2$, an increase of the tunneling current occurs once the tip crosses the paraboloid. Accordingly, dI/d$V(X, Y)$ maps exhibit a ring centered to the molecule (Fig. 2h), whereby the diameter depends on V_s. This is represented by the series of concentric rings inside the paraboloid shown in Fig. 2g. Inside the ring (Fig. 2h), the tip field induces the molecule's discharge by one electron (region $e = 1$), while outside the ring no charge is being removed ($e = 0$). Note finally that neutral TBTAP^0 molecules have no electrons sensitive to such discharging process observed for positive sample voltages. Thus, no such rings are visible at their positions in dI/dV maps.

Reversible discharge by capacitive coupling with the tip

To shed light into the capacitive character of the discharge process, we employed dI/d$V(V)$ and $\Delta f(V)$ spectroscopic measurements as a function of the tip-sample separation Z. Fig. 3a and b show an exemplary STM image of the assembly at V_s = 1.2 V and the corresponding constant-height dI/dV maps. Rings and dots of high conductance are unambiguously resolved centered on each TBTAP$^{\bullet -}$ molecule of c rows. The constant-height $\Delta f(X, Y)$ map of Fig. 3c acquired at the same sample location reveals similar ring features, which demonstrates the successful control of the molecule's discharge using an AFM.[27,43,45–47] The rings have a dark contrast as compared to the gray background in the AFM image,[27,43,45–47] because discharging events are associated to a dip in $\Delta f(V)$ curves (Fig. 3e) in contrast to a peak in tunneling spectra (Fig. 3d).

Fig. 3d and e show the typical signature of the discharge denoted V^* in a series of dI/d$V(V)$ and $\Delta f(V)$ spectra for increasing tip-sample separations Z. In dI/dV ($\Delta f(V)$) spectra, the discharge is observed as a peak (dip) marked by an arrow. Their positions in voltage correspond to the discharge threshold ($V_{-\rightarrow 0}$) and varies between 0.8 up to 1.3 V. By gradually increasing the tip-sample separation Z, we observe that these occurrences shift towards higher voltage values in both dI/dV and $\Delta f(V)$ spectra. To better visualize this dependency, Fig. 3f shows a plot of V^* extracted from the dI/dV (red) and $\Delta f(V)$ (blue) spectra as a function of the relative tip-height Z.

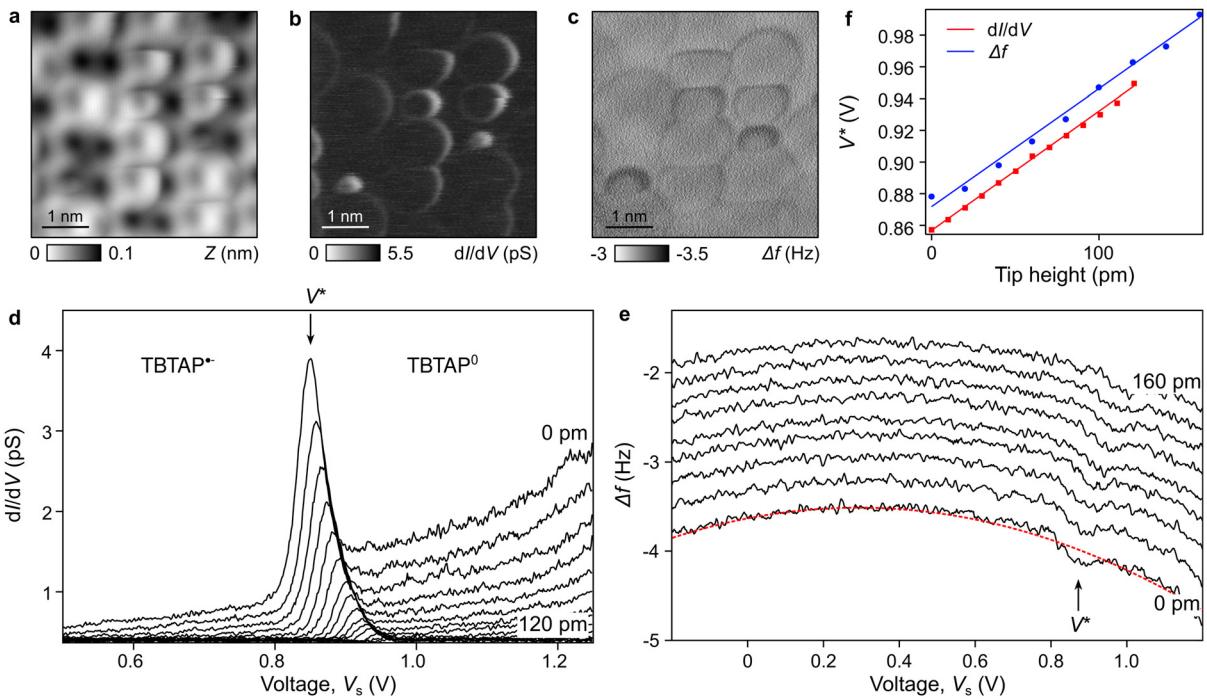

Fig. 3 Gating efficiency of radical TBTAP$^{\bullet -}$ with the tip. (a) STM topographic image of the TBTAP assembly (V_s = 1.2 V, I_t = 1 pA). (b) and (c) Constant-height dI/dV maps and $\Delta f(X, Y)$ map acquired at V = 1.2 V at the same position showing the Coulomb rings. (d) and (e) Series of dI/dV(V) and $\Delta f(V)$ point-spectra acquired above a TBTAP$^{\bullet -}$ molecule for increasing the tip-sample separation Z. Peaks (dips) in the dI/dV(Δf) spectra denoted V^* indicates the discharge of the molecule induced by the electric field of the tip as a function of the tip-sample separation Z. (f) Plot of V^* as a function of Z from tunneling (red) and force (blue) spectroscopic measurements of (d) and (e) showing the linearly shift of V^* towards higher values as Z increases. This linear progression is characteristic of the capacitive coupling between the tip field and the charged molecule.

To extract the dips in $\Delta f(V)$, we first extracted the local contact potential difference (LCPD) by fitting a parabola (red curve),[21] which was then subtracted from raw data as described in ref. 43. Using a Gaussian function, we then extracted the voltage positions of each discharging event. The red and blue lines in Fig. 3f are fits of both tunneling and force datasets. They clearly show the linear progression of V^* as a function of Z, in agreement with the capacitive character of the discharge process induced by the tip field. Although the relative tip height Z determined by the STM setpoint is identical for both datasets, the fits are laterally shifted in voltage by $\approx$ 20 mV with respect to each other. We think that this arises from the oscillation of the sensor ($A_{osc} \approx 50$ pm) needed for force spectroscopic measurements, which induces an effective Z offset as compared to the dI/d$V(V)$ measurements. Indeed, despite using the same tip-sample separation Z, the Δf map of Fig. 3c shows slightly larger Coulomb rings as compared to those of the dI/dV map.

Cascade discharge and electron correlation in the supramolecular assembly

We next investigated the spatial distribution of Coulomb rings within the supramolecular assembly as a function of the voltage V_s in a series of dI/dV maps (Fig. 4). As schematized in Fig. 4a, the discharge of neighboring TBTAP$^{\bullet -}$ molecules acting as quantum dots follows a voltage-dependent paraboloid shape centered to each molecule. Fig. 4b shows an experimental dI/d$V(X, V)$ cross-section acquired along two radical molecules of a c row. The dashed lines mark the positions X of the molecule's center, relative to which parabolas are centered. The gray line marks the line-shape of the discharge voltage V^*, which value depends on the lateral position of the tip with respect to the molecules. The parabola branches linearly expand as V_s increases and fuse at about $V_s = V_2 = 1.2$ V when the tip is located between neighboring molecules. At this crossing point, the tip discharges the two molecules at the same time. This observation is similar to the work by Li *et al.* showing in dI/dV maps complex Coulomb patterns from correlated electrons in WS_2/WSe_2 moiré superlattices.[8] The electron correlation is schematized in Fig. 4a by considering a non-null hopping amplitude t between two coupled Coulomb-blockaded molecular QD with on-site Coulomb interaction U. At $V_s \geq V_2$, the parabola shown with plain lines merge implying a cascade discharge, which can be visualized in two-dimensional dI/d$V(X, Y)$ maps in the forms of fused Coulomb rings (depicted in red in Fig. 4a).

Fig. 4d–f show a series of dI/dV(X, Y) maps at various voltages at the area shown in the topographic STM image of Fig. 4c. For $V_s = 1$ V, a periodic pattern of dots starts to appear at molecules of c rows. Increasing V_s from 1.15 V to 1.3 V (Fig. 4e and f) leads to the appearance of additional rings as well as an increase of their diameters. At $V_s = 1.15$ V, rings start to overlap as their radii are almost equal to the intermolecular distance. For $V_s = V_2 = 1.3$ V (Fig. 4f), the dI/dV map shows the coalescence of these rings along c rows. This observation differs from patterns with intersecting rings as expected from a non-interacting scenario, similar to that for the case of anionic

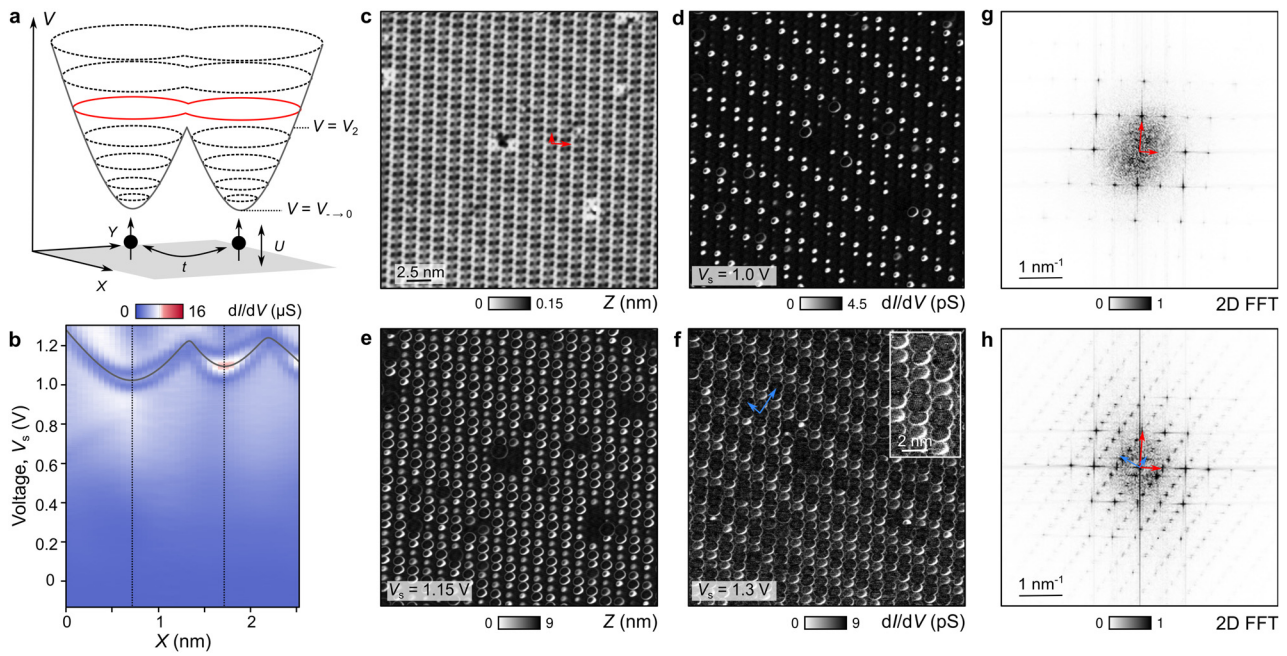

Fig. 4 Imaging cascade discharge and electron correlation of the supramolecular lattice. (a) Schematic of two interacting quantum dots with on-site Coulomb interaction U and hopping integral t, which can be discharged by the tip when $V_s \geq V_{-\rightarrow 0}$. At $V_s = V_2$, the parabola centered to each QD start crossing leading to the fusion of the Coulomb rings in dI/dV maps. (b) Experimental dI/d$V(X, V)$ cross-section acquired across three charged molecules. Each parabola is centered to the position of the TBTAP$^{\bullet -}$ molecules, which merges at $V_s \approx 1.2$ V. (c) Topographic STM image of the TBTAP assembly ($I_t = 1$ pA, $V_s = 0.5$ V). (d)–(f) Series of dI/dV maps at sample voltage $V_s = 1.0$ V, 1.15 V and 1.3 V, respectively. The inset of f is a zoom showing the fused rings. (g) and (h) 2D fast-Fourier transform (2D-FFT) extracted from the TBTAP assembly of (c) (red arrows) and of the Coulomb pattern of (f) (blue arrows).

TBTAP$^{\bullet-}$ on Ag(111).[19] Thus, it represents an experimental manifestation of the electron correlation in the supramolecular assembly.

For $V_s \geq 1.3$ V, the two-dimensional Coulomb superlattice emerges in the dI/dV map. We used 2D-fast Fourier transform (2D-FFT) to compare the rectangular supramolecular lattice of parameters $1/a_1 = 0.81$ nm^{-1} ($a_1 = 12.3$ Å) and $1/b_1 = 0.53$ nm^{-1} ($b_1 = 18.9$ Å) (red arrows of Fig. 4c and g) with the charge superlattice of $1/a_2 = 0.25$ nm^{-1} ($a_2 = 40$ Å) and $b_2 = 0.5$ nm^{-1} ($b_2 = 20$ Å) rotated by 45° (blue arrows of Fig. 4f and h). We infer this charge superlattice to a slight modulation of the surface potential induced by the commensurability of the molecular lattice with the substrate.

Irreversible discharge of TBTAP$^{\bullet-}$ molecules induced by tip chemistry

To probe ring fusing between neighboring c rows, gating voltages V_s greater than 1.5 V should be employed for the dI/dV maps. However, we found out that such high voltages also lead to cleavage of the C-Br bonds of the TBTAP molecule,[48] making this experiment inconclusive. We next used this controlled tip chemistry protocol to fabricate single defects in the supramolecular lattice. Fig. 5a and b show a typical topographic STM image of the molecular network and the corresponding constant-height dI/dV map at $V_s = 1.0$ V revealing the charged superlattice. A short voltage pulse of about 10–100 ms ($V_s = 2.0$ V) was applied at the red dot of Fig. 5a, which induces a change of contrast in the subsequent STM image of Fig. 5c. The corresponding constant-height dI/dV map at $V_s = 1.0$ V (Fig. 5d) confirms the disappearance of one Coulomb ring as pointed out by an yellow arrow. As a result of this modification, the electron (spin) of the pristine TBTAP$^{\bullet-}$ molecule is irreversibly removed turning the molecule into a neutral state. This is also confirmed by comparing dI/dV point-spectra (Fig. 5f) before (red) and after (blue) the tip pulse, showing the disappearance of the YSR sub-gap states at $\pm\varepsilon$ energies originally present in the TBTAP$^{\bullet-}$ molecule. The comparison of Fig. 5b and c near the pulse position also reveals that few discharge rings appear smaller than before the voltage pulse. We think that this phenomenon results from the controlled creation of such a defect within the charge superlattice, which may modify the modulation of the surface potential defined by the molecular lattice on Pb. This can influence the discharge threshold of the neighboring radical molecule, leading to a decrease in the size of the ring in dI/dV maps.

Fig. 5g shows the DOS of TBTAP$^{\bullet-}$ obtained by DFT calculations. At 1.8 eV above E_F, the presence of C-Br states indicates that splitting off one of the Br atoms from the tetraazapyrene backbone is induced by tunneling into them during the voltage pulse. DFT calculations of the debrominated TBTAP DOS (Fig. 5h)

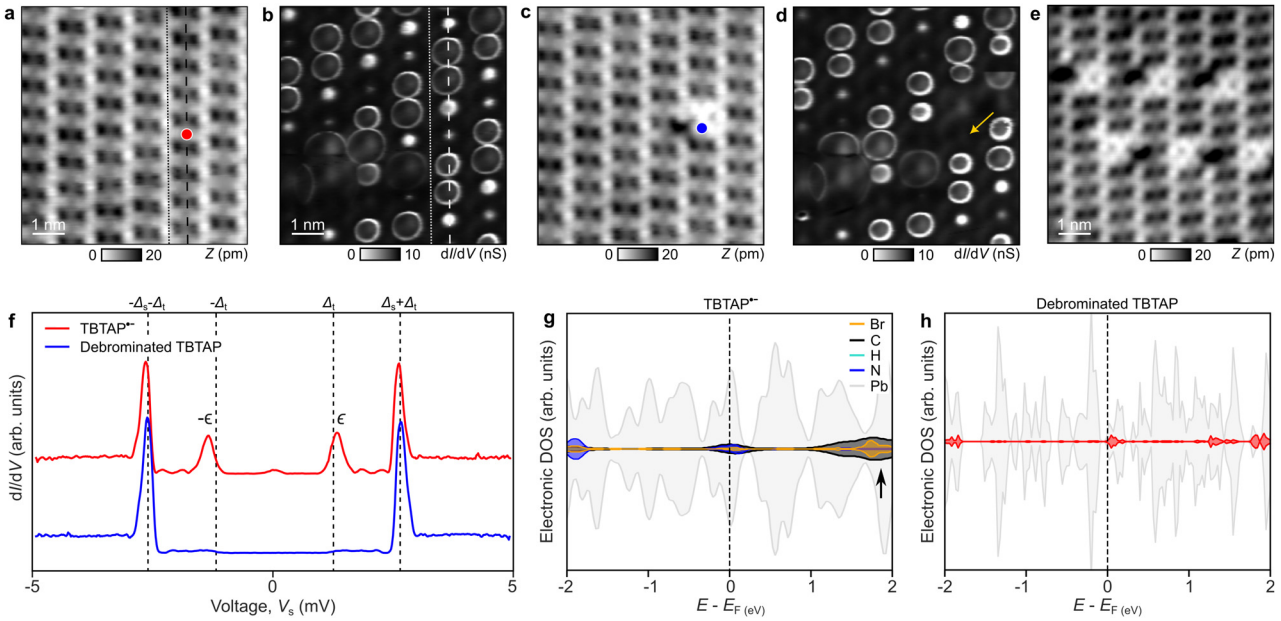

Fig. 5 Irreversible discharge of TBTAP$^{\bullet-}$ induced by tip chemistry. (a) STM image of the TBTAP assembly ($I_t = 1$ pA, $V_s = 50$ mV). The dashed and dotted lines labeled c and n correspond to rows of charged and neutral TBTAP molecules. The red dot marks the position where a short (10–100 ms) voltage pulse of about 1.8 V has been applied, leading to debromination of the molecule. (b) Constant-height dI/dV map at $V_s = 1.0$ V at the same position showing the Coulomb pattern before debromination. (c) STM image of the TBTAP assembly after debromination ($I_t = 1$ pA, $V_s = 50$ mV) and, (d) Corresponding constant-height dI/dV map at $V_s = 1.0$ V revealing the removal of one coulomb ring of the charge superlattice (yellow arrow). (e) Example of a simple defect pattern constructed in the TBTAP assembly by tip chemistry. (f) dI/dV point-spectra acquired at the red (blue) dots of a (c) with a superconducting Pb tip (lock-in parameters: $f = 611$ Hz, $A_{mod} = 20$ μV, tunneling parameters: $I_t = 100$ pA, $V_s = 5$ mV). Dashed lines correspond to $\pm(\Delta_t + \Delta_s)$ and $\pm\Delta_t$ with Δ_t and Δ_s are the superconducting gap of tip and sample, respectively. Before debromination, the TBTAP$^{\bullet-}$ radical has one pair of YSR sub-gap states at the $\pm\varepsilon$ energies due to its $S = 1/2$ electron spin. The YSR states vanish after debromination proving the electron (spin) removal and its neutral state. (g) Electronic DOS of the TBTAP$^{\bullet-}$ molecule showing the C–Br states at about 1.8 eV above E_F. (h) Electronic DOS of the debrominated TBTAP showing a completely empty LUMO.

also confirm the shift of the molecular LUMO by about 0.1 eV above E_F leading to a completely unoccupied LUMO as expected for a neutral molecule. This controlled tip chemistry is reproducible as shown in Fig. 5e and thus offers an exciting prospect to create complex patterns and topological states by local probe chemistry in a supramolecular electron spin array.[49] This will be addressed in details in a future work.

Conclusion

In summary, the spontaneous assembly of TBTAP molecules on superconducting Pb(111) forms a compact electron (spin) superlattice with coexisting neutral TBTAP and singly-charged $TBTAP^{\bullet-}$ molecules. Using $dI/dV(V)$ and force-voltage spectroscopy $\Delta f(V)$ spectroscopic measurements, we demonstrate controlled and reversible discharging of anionic $TBTAP^{\bullet-}$ *via* capacitive coupling between the STM/AFM tip and the singly-occupied molecular state. This tip-induced transition from an anionic to neutral state is further visualized in spatial dI/dV maps as a pattern of Coulomb rings centered on charged molecules. At higher gating voltages, these rings merge, indicating cascade discharge events and strong electron correlation across the molecular lattice. Furthermore, we employ tip-induced chemistry to selectively debrominate individual $TBTAP^{\bullet-}$ molecules, causing an irreversible transition to the neutral state and enabling the controlled introduction of defects within the supramolecular lattice. These findings establish a platform for the bottom-up design of gate-tunable electron spin arrays with ultrahigh areal density, offering promising avenues for future applications in quantum computing and quantum sensing.

Author contributions

R. P., S.-X. L., S. D. and E. M. conceived the experiments. X. L., R. H., S.-X. L. and S. D. synthesized the precursors. C. D., C. L., J.-C. L., and R. P. performed the STM/AFM measurements. U. A. performed DFT calculations. C. D., C. L. and R. P. analyzed the data. C. D. and R. P. wrote the manuscript. All authors discussed on the results and revised the manuscript.

Conflicts of interest

The authors declare no competing financial interests.

Data availability

All images and spectra presented in this article are raw data. The data are available in Zenodo at **https://doi.org/10.5281/zenodo.15805067**.

Acknowledgements

We gratefully acknowledge the Werner Siemens Stiftung (WSS) for supporting the WSS Research Center for Molecular Quantum Systems (molQ). E. M. and R. P. acknowledge funding from the Swiss Nanoscience Institute (SNI) and the European Research Council (ERC) under the European Unions Horizon 2020 research and innovation programme (ULTRADISS grant agreement No. 834402) and supports as a part of NCCR SPIN, a National Centre of Competence (or Excellence) in Research, funded by the SNF (grant number 51NF40-180604). E. M. and S.-X. L. acknowledge the Sinergia Project funded by the SNF (CRSII5_213533). E. M. and R. P. acknowledge the SNF grant (200021_228403). S.-X. L. acknowledges the grant from the SNF (200021_204053). U. A. acknowledges funding by the SNF Professorship (Grant No. PP00P2 187185/2). Calculations were performed using supercomputer resources provided by the Vienna Scientific Cluster (VSC). C. L. acknowledges the Georg H. Endress Foundation for financial support.

References

1 M. Oh, K. P. Nuckolls, D. Wong, R. L. Lee, X. Liu, K. Watanabe, T. Taniguchi and A. Yazdani, *Nature*, 2021, **600**, 240–245.
2 Y. Xu, S. Liu, D. A. Rhodes, K. Watanabe, T. Taniguchi, J. Hone, V. Elser, K. F. Mak and J. Shan, *Nature*, 2020, **587**, 214–218.
3 E. C. Regan, D. Wang, C. Jin, M. I. Bakti Utama, B. Gao, X. Wei, S. Zhao, W. Zhao, Z. Zhang, K. Yumigeta, M. Blei, J. D. Carlström, K. Watanabe, T. Taniguchi, S. Tongay, M. Crommie, A. Zettl and F. Wang, *Nature*, 2020, **579**, 359–363.
4 L. Wang, E.-M. Shih, A. Ghiotto, L. Xian, D. A. Rhodes, C. Tan, M. Claassen, D. M. Kennes, Y. Bai, B. Kim, K. Watanabe, T. Taniguchi, X. Zhu, J. Hone, A. Rubio, A. N. Pasupathy and C. R. Dean, *Nat. Mater.*, 2020, **19**, 861–866.
5 J. P. Dehollain, U. Mukhopadhyay, V. P. Michal, Y. Wang, B. Wunsch, C. Reichl, W. Wegscheider, M. S. Rudner, E. Demler and L. M. K. Vandersypen, *Nature*, 2020, **579**, 528–533.
6 C. Gross and I. Bloch, *Science*, 2017, **357**, 995–1001.
7 A. Mazurenko, C. S. Chiu, G. Ji, M. F. Parsons, M. Kanász-Nagy, R. Schmidt, F. Grusdt, E. Demler, D. Greif and M. Greiner, *Nature*, 2017, **545**, 462–466.
8 H. Li, S. Li, M. H. Naik, J. Xie, X. Li, E. Regan, D. Wang, W. Zhao, K. Yumigeta, M. Blei, T. Taniguchi, K. Watanabe, S. Tongay, A. Zettl, S. G. Louie, M. F. Crommie and F. Wang, *Nat. Phys.*, 2021, **17**, 1114–1119.
9 X. Wang, E. Khatami, F. Fei, J. Wyrick, P. Namboodiri, R. Kashid, A. F. Rigosi, G. Bryant and R. Silver, *Nat. Commun.*, 2022, **13**, 6824.
10 J. Salfi, J. A. Mol, R. Rahman, G. Klimeck, M. Y. Simmons, L. C. L. Hollenberg and S. Rogge, *Nat. Commun.*, 2016, **7**, 11342.
11 T. Hensgens, T. Fujita, L. Janssen, X. Li, C. J. Van Diepen, C. Reichl, W. Wegscheider, S. Das Sarma and L. M. K. Vandersypen, *Nature*, 2017, **548**, 70–73.
12 M. Fuechsle, J. A. Miwa, S. Mahapatra, H. Ryu, S. Lee, O. Warschkow, L. C. L. Hollenberg, G. Klimeck and M. Y. Simmons, *Nat. Nanotechnol.*, 2012, **7**, 242–246.

13 M. Kiczynski, S. K. Gorman, H. Geng, M. B. Donnelly, Y. Chung, Y. He, J. G. Keizer and M. Y. Simmons, *Nature*, 2022, **606**, 694–699.
14 A. A. Khajetoorians, D. Wegner, A. F. Otte and I. Swart, *Nat. Rev. Phys.*, 2019, **1**, 703–715.
15 Y. He, S. K. Gorman, D. Keith, L. Kranz, J. G. Keizer and M. Y. Simmons, *Nature*, 2019, **571**, 371–375.
16 J. Repp, G. Meyer, F. E. Olsson and M. Persson, *Science*, 2004, **305**, 493.
17 X. H. Qiu, G. V. Nazin and W. Ho, *Phys. Rev. Lett.*, 2004, **92**, 206102.
18 D. Kumar, C. Krull, Y. Yin, N. V. Medhekar and A. Schiffrin, *ACS Nano*, 2019, **13**, 11882–11890.
19 C. Li, C. Kaspar, P. Zhou, J. Liu, O. Chahib, T. Glatzel, R. Häner, U. Aschauer, S. Decurtins, S. Liu, M. Thoss, E. Meyer and R. Pawlak, *Nat. Commun.*, 2023, **14**, 5956.
20 M. T. Woodside and P. L. McEuen, *Science*, 2002, **296**, 1098–1101.
21 R. Stomp, Y. Miyahara, S. Schaer, Q. Sun, H. Guo, P. Grutter, S. Studenikin, P. Poole and A. Sachrajda, *Phys. Rev. Lett.*, 2005, **94**, 056802.
22 L. Gross, F. Mohn, P. Liljeroth, J. Repp, F. J. Giessibl and G. Meyer, *Science*, 2009, **324**, 1428–1431.
23 W. Steurer, J. Repp, L. Gross, I. Scivetti, M. Persson and G. Meyer, *Phys. Rev. Lett.*, 2015, **114**, 036801.
24 G. Chen, R.-J. Sun, D.-B. Wang, W.-A. Liao, W.-H. Zhang, C.-F. Liu and Y.-S. Fu, *J. Am. Chem. Soc.*, 2025, **147**, 12949–12955.
25 W. Steurer, S. Fatayer, L. Gross and G. Meyer, *Nat. Commun.*, 2015, **6**, 8353.
26 S. Fatayer, B. Schuler, W. Steurer, I. Scivetti, J. Repp, L. Gross, M. Persson and G. Meyer, *Nat. Nanotechnol.*, 2018, **13**, 376–380.
27 P. Scheuerer, L. L. Patera and J. Repp, *Nano Lett.*, 2020, **20**, 1839–1845.
28 C. Wagner, M. F. Green, P. Leinen, T. Deilmann, P. Krüger, M. Rohlfing, R. Temirov and F. S. Tautz, *Phys. Rev. Lett.*, 2015, **115**, 026101.
29 J. Berger, M. Ondráček, O. Stetsovych, P. Malý, P. Holý, J. Rybáček, M. Švec, I. G. Stará, T. Mančal, I. Starý and P. Jelínek, *Nat. Comm.*, 2020, **11**, 1337.
30 I. Fernández-Torrente, D. Kreikemeyer-Lorenzo, A. Stróżecka, K. J. Franke and J. I. Pascual, *Phys. Rev. Lett.*, 2012, **108**, 036801.
31 K. Regos, R. Pawlak, X. Wang, E. Meyer, S. Decurtins, G. Domokos, K. S. Novoselov, S.-X. Liu and U. Aschauer, *Proc. Nat. Acad. Sci. U. S. A.*, 2023, **120**, e2300049120.
32 S. L. Bayliss, D. W. Laorenza, P. J. Mintun, B. D. Kovos, D. E. Freedman and D. D. Awschalom, *Science*, 2020, **370**, 1309–1312.
33 C. Li, V. Pokorný, M. Žonda, J.-C. Liu, P. Zhou, O. Chahib, T. Glatzel, R. Häner, S. Decurtins, S.-X. Liu, R. Pawlak and E. Meyer, *ACS Nano*, 2025, **19**, 3403–3413.
34 P. Zhou, U. Aschauer, S. Decurtins, T. Feurer, R. Häner and S.-X. Liu, *Chem. Commun.*, 2021, **57**, 12972–12975.
35 F. J. Giessibl, *Rev. Sci. Instr.*, 2019, **90**, 011101.
36 J. VandeVondele, M. Krack, F. Mohamed, M. Parrinello, T. Chassaing and J. Hutter, *Comp. Phys. Commun.*, 2005, **167**, 103–128.
37 T. D. Kühne, M. Iannuzzi, M. Del Ben, V. V. Rybkin, P. Seewald, F. Stein, T. Laino, R. Z. Khaliullin, O. Schütt, F. Schiffmann, D. Golze, J. Wilhelm, S. Chulkov, M. H. Bani-Hashemian, V. Weber, U. Borštnik, M. Taillefumier, A. S. Jakobovits, A. Lazzaro, H. Pabst, T. Müller, R. Schade, M. Guidon, S. Andermatt, N. Holmberg, G. K. Schenter, A. Hehn, A. Bussy, F. Belleflamme, G. Tabacchi, A. Glöß, M. Lass, I. Bethune, C. J. Mundy, C. Plessl, M. Watkins, J. VandeVondele, M. Krack and J. Hutter, *J. Chem. Phys.*, 2020, **152**, 194103.
38 Y. Zhang and W. Yang, *Phys. Rev. Lett.*, 1998, **80**, 890.
39 S. Grimme, J. Antony, S. Ehrlich and H. Krieg, *J. Chem. Phys.*, 2010, **132**, 154104.
40 J. VandeVondele and J. Hutter, *J. Chem. Phys.*, 2007, **127**, 114105.
41 S. Goedecker, M. Teter and J. Hutter, *Phys. Rev. B: Condens. Matter Mater. Phys.*, 1996, **54**, 1703–1710.
42 R. Pawlak, J.-C. Liu, C. Li, R. Hess, H. Chen, C. Drechsel, P. Zhou, R. Häner, U. Aschauer, T. Glatzel, S. Decurtins, D. Loss, J. Klinovaja, S.-X. Liu, W. Wulfhekel and E. Meyer, Towards Gate-Tunable Topological Superconductivity in a Supramolecular Electron Spin Lattice, 2025, **https://arxiv.org/abs/2310.18134**.
43 N. Kocić, P. Weiderer, S. Keller, S. Decurtins, S.-X. Liu and J. Repp, *Nano Lett.*, 2015, **15**, 4406–4411.
44 G. V. Nazin, X. H. Qiu and W. Ho, *Phys. Rev. Lett.*, 2005, **95**, 166103.
45 L. Cockins, Y. Miyahara, S. D. Bennett, A. A. Clerk, S. Studenikin, P. Poole, A. Sachrajda and P. Grutter, *Proc. Nat. Acad. Sci. U. S. A.*, 2010, **107**, 9496–9501.
46 N. Kocić, S. Decurtins, S.-X. Liu and J. Repp, *J. Chem. Phys.*, 2017, **146**, 092327.
47 N. Kocić, D. Blank, P. Abufager, N. Lorente, S. Decurtins, S.-X. Liu and J. Repp, *Nano Lett.*, 2019, **19**, 2750–2757.
48 Q. Zhong, A. Ihle, S. Ahles, H. A. Wegner, A. Schirmeisen and D. Ebeling, *Nat. Chem.*, 2021, **13**, 1133–1139.
49 S. Kawai, O. Krejčí, T. Nishiuchi, K. Sahara, T. Kodama, R. Pawlak, E. Meyer, T. Kubo and A. S. Foster, *Sci. Adv.*, 2020, **6**, eaay8913.